Revision 2

Iron sulfide stoichiometry as a monitor of sulfur fugacity in gas-mixing experiments

ASTRID HOLZHEID[1] AND KATHARINA LODDERS[2]

[1] Institut für Geowissenschaften, Universität Kiel, 24098 Kiel, Germany,
E-mail: holzheid@min.uni-kiel.de

[2] Planetary Chemistry Laboratory, Department of Earth and Planetary Sciences and McDonnell Center for the Space Sciences, Washington University, Campus Box 1169, One Brookings Drive, St. Louis, MO 63130-4899, USA, E-mail: lodders@wustl.edu

submitted 10/08/2012 to *American Mineralogist,* revised 04/04/2013

ABSTRACT

We explore a method to utilize the stoichiometry of iron sulfide to determine the sulfur fugacity in experiments containing CO-CO_2-SO_2 gas mixtures. The Fe-S phase diagram shows that the stoichiometry of iron sulfide melts is closely related to the sulfur fugacity fS_2 at a given temperature and ambient pressure. We derive equations that relate the sulfur fugacity to the mole fraction of sulfur X_S in the iron sulfide from available literature data, and a solution model using the Redlich-Kister approximation for the excess Gibbs energy of mixing. We test the method by exposing iron sulfide to CO-CO_2-SO_2 gas mixtures and subsequently analyzing the "Fe-S monitor" for its stoichiometry. Most sulfur fugacities calculated from the equilibrium gas composition agree within 5-10% (1200°C) and 1-4% (1400°C) with those derived from the sulfur mole fraction in the monitor

and literature data calibration, which is consistent with the spread observed in literature data. There were no suitable literature data for a full calibration at 1300°C, so we combined the available literature and our data to find the sulfur fugacity as a function of mole fraction sulfur. Overall the Fe-S monitor technique is a convenient method to determine the sulfur fugacity in high temperature experiments containing CO-CO_2-SO_2 gas mixtures as long as oxygen fugacities remain below that of the iron-wüstite or iron-magnetite buffer.

Keyword: iron sulfide, stoichiometry, sulfur fugacity, fS_2 monitor

INTRODUCTION

Sulfur plays an important role in metallurgical, environmental, geochemical and cosmochemical processes. The sulfur fugacity (fS_2) is a fundamental parameter in many applications. Sulfur is a common contaminant in exhaust gases from ore processing plants and smelters. Thermodynamic models of volcanic gas compositions on Earth, on Jupiter's volcanically active moon Io, and possibly on Venus, use the sulfur fugacity as key parameter to evaluate the abundance of sulfur-bearing gases such as SO, SO_2, and COS (see Lodders and Fegley 1998; Fegley 2013). The sulfur fugacity influences the solubility limit of sulfur in silicate magmas (e.g., Poulson and Ohmoto 1990) and is important for modelling the genesis of sulfide ores that are associated with mafic and ultramafic igneous rocks (e.g., Mungall and Naldrett, 2008, and references therein). Models of planetary differentiation and core formation rely on experimentally determined major and trace element partition coefficients between coexisting metal, metallic sulfides, and/or (liquid) silicates. These partition coefficients depend on the oxygen and sulfur fugacities. Numerous studies of elemental metal/silicate partitioning as function of oxygen fugacity are available (see Walter et al.

(2000) and Righter (2003) for literature reviews up to 1999 and 2002, respectively; more recent experimental studies on metal/silicate partitioning are e.g., Holzheid and Palme 2007; Corgne et al. 2008; Kegler et al. 2008; Cottrell et al. 2009; Mann et al. 2009; Cottrell et al. 2010; Siebert et al. 2011; Bouhifd and Jephcoat 2011; Kegler and Holzheid 2011; Righter 2011; Palme et al. 2011; Siebert et al. 2012).

Metal/sulfide and liquid silicate/sulfide partitioning data at ambient and elevated pressures are limited (see e.g., Chabot and Jones (2003) and Chabot et al. (2003) for compilation of experimental studies on metal/sulfide partition coefficients; for liquid silicate/sulfide partitioning data see e.g., Li and Agee (1996); Peach and Mathez (1993); Bezmen et al. (1994) and references therein).

Results from experimental studies can be used to model element distributions between coexisting metal, sulfide, and silicates provided that the temperature T, total pressure P, oxygen fugacity fO_2, and sulfur fugacity fS_2, are well known for the experiments. Temperatures for experiments above 1000°C are routinely measured with $PtRh_6/PtRh_{30}$ or other alloy thermocouples, and the fO_2 is measured commonly with CaO-Y_2O_3-doped ZrO_2 solid electrolyte sensors.

Sulfur-bearing experimental setups can be done in two ways. One way is equilibration of experimental charges in evacuated sealed silica tubes (e.g., Lodders and Palme 1991). In such experiments, the fO_2- and fS_2-values can only be derived from the compositions of the phase assemblages after the experiment. The other way to impose controlled sulfur fugacities is to use H_2-H_2S gas mixtures or, for additional control of oxygen fugacities, CO-CO_2-SO_2 gas mixtures. We employed the latter method to study trace element partitioning between metal, iron sulfide, and silicate (Holzheid and Lodders 2001). The advantage of using CO-CO_2-SO_2 gas mixtures is that fO_2 and fS_2 are simultaneously superimposed on the experimental charges and are easily varied to the desired values. The fO_2- and fS_2-values for CO-CO_2-SO_2 gas mixtures at or near ambient pressure

70 are calculated from thermodynamic properties (e.g., Chase 1998; Gurvich et al. 1989; see below) for
71 the various coexisting gas species in the CO-CO_2-SO_2 system. The fO_2 can also be directly measured
72 with CaO-Y_2O_3-doped ZrO_2 solid electrolyte sensors. For experimental charges consisting of metal
73 and silicate, the fO_2 can be calculated from the Fe content of the metal phase and FeO content of the
74 silicate after the experiment. Therefore, three independent methods to determine the fO_2 are
75 available.

76 Solid electrolyte based sulfur fugacity sensors are only available for operation at room
77 temperature or within the temperature range of 500°C to 950°C (e.g., Gauthier et al. 1977;
78 Maruyama et al. 1985; Saito et al. 1986; Maruyama 1991). There are no readily available solid
79 electrolyte sensors for measuring fS_2 at T>1000°C. Thus, the fS_2 must be calculated from the
80 chemical equilibrium composition of the high T gas mixture or be determined from the resulting
81 phase assemblages. The latter requires that the experimental charges are relatively simple in
82 composition, e.g., "pure" iron sulfide, Fe-metal, and FeO-bearing silicates for which the activity of
83 "FeO" is known. The derivation of the fS_2 from the composition of phase assemblages becomes
84 complex in multi-component alloy systems such as Fe-Co-Ni-S-alloys if the required phase relations
85 and/or activity coefficients are not known. If coexisting metal or sulfide phases are absent, the
86 determination of fS_2 is very difficult for pure silicate systems, because sulfur solubilities in melts
87 depend on overall melt composition. To circumvent these obstacles, we explored a relatively simple
88 and robust method to monitor the sulfur fugacity for experiments done in CO-CO_2-SO_2 gas mixtures
89 by using the composition of an iron sulfide monitor. The bulk sulfur content of the monitor will
90 change by either losing or gaining sulfur, depending on the initial composition of the iron sulfide
91 used and the superimposed sulfur fugacity.

This paper is organized as follows. We start with experimental details, including calculation procedure of oxygen and sulfur fugacities and the determination of the bulk sulfur content of the Fe-S monitor after the experiments. This is followed by a detailed discussion of the Fe-S monitor concept, a comparison of various methods to determine oxygen and sulfur fugacities, and concluding remarks.

FE-S MONITOR EXPERIMENTS

Equilibration procedure

All run parameters are summarized in Table 1. Commercial FeS-powder (metal basis, 99.99%, Alfa Chemicals) with known stoichiometry was used in all experiments. The commercial FeS has X_S = 0.501 as calculated from the manufacturer's analysis and X_S = 0.504 from four combustion analyses done here (method described below). In addition, synthetic FeS-powder, manufactured from Fe-metal in our laboratory at Washington University, was used in three experiments to test agreement of the fS_2 determination by use of iron sulfide with different initial Fe/S-ratios. In initial experiments pure Fe powder was used instead of FeS powder to monitor the fS_2 but the kinetics of iron sulfidation is too slow at even 1300°C and the metallic iron did not react completely to iron sulfide as expected for the given fS_2. This problem did not exist when iron sulfide was used as a monitor. Time series experiments at 1300°C and 1400°C have shown that X_S of the iron sulfide remained constant under similar oxygen and sulfur fugacities for run durations longer than 24 hours. Therefore only experiments with iron sulfide as monitor and run durations of more than 24 hours, including the time series experiments, are listed in Table 1.

The iron sulfide powder (50 - 660 mg total), inserted into a small corundum crucible (length 10 mm, ID 6 mm), was placed together with up to five other samples of interest into the isothermal hot

zone of Deltech vertical tube furnaces at one atmosphere under different oxygen and sulfur fugacities, and temperatures (see Holzheid and Lodders (2001) for more details). Run durations varied between 24 and 94 hours. Oxygen and sulfur fugacities in the S-bearing experiments were controlled by CO-CO_2-SO_2 gas mixtures. The temperature and oxygen fugacity were measured with a $PtRh_6/PtRh_{30}$ thermocouple and a CaO-Y_2O_3-stabilized ZrO_2 solid electrolyte sensor, respectively. All samples were quenched by withdrawing the charge rapidly from the hot zone to the cooler top of the furnace while still in the gas mixture. The samples were allowed to cool to about 100°C prior to removal from the furnace, so that oxidation in air was prevented.

The use of CO-CO_2-SO_2 gas mixtures also imposes an oxygen fugacity onto the Fe-S monitor which could lead to oxidation of the Fe-S monitor and limit its usefulness.

Indeed, Nagamori and Kameda (1965) showed at log fO_2 of IW+0.7 up to 10 mass% oxygen in Fe-S phases. The oxygen fugacities in our experiments were below that of the iron-wüstite or iron-magnetite buffer (depending on temperature). An indication that no oxidation of the Fe-S monitor occurred during the calibration in the CO-CO_2-SO_2 gas mixtures is that several of our monitor samples that were equilibrated at our highest oxygen fugacities show good agreement with the expected monitor compositions from the literature calibrations. Furthermore X-ray diffraction of a set of Fe-S monitor samples after the experiment did not show any diffraction pattern signatures that would indicate a larger amount of wüstite or magnetite (> 1-2 vol.%). We are confident that no significant oxidation, if any, of the Fe-S monitor occurred.

Calculation of oxygen and sulfur fugacities in CO-CO_2-SO_2 gas mixtures from thermodynamic data

The sulfur and oxygen fugacities at run temperatures were calculated from thermodynamic data and the mixing ratios of the incoming CO-CO_2-SO_2 gas. Two sets of calculations were done, each using a self-consistent set of thermodynamic data from either the JANAF tables (Chase et al. 1998) or the data compilation by Gurvich et al. (1989) to check uncertainties in fO_2 and fS_2 introduced by thermodynamic data. The compounds considered in both sets of calculations are the gases CO, CO_2, S, S_2, S_3, S_4, S_5, S_6, S_7, S_8, SO, SO_2, SO_3, S_2O, CS, CS_2, COS, O, O_2, O_3, and solid graphite (reference state of carbon). The fO_2, fS_2, and the graphite activity ($a_{graphite}$) are solved from a set of non-linear equations that can be written from the formation reactions and equilibrium constants of each compound in the system from the elements in their reference state. This is a standard procedure as frequently done for gas and solid equilibria (e.g., Lodders 2003).

It is noted that data for S_2O (g) (and those of some other S-bearing gases) in JANAF are erroneous (see Lodders 2004) and that corrected data were used in the computations. The mixing ratios of CO, CO_2, and SO_2 and the fO_2 and fS_2 calculated from both Chase et al. (1998) and Gurvich et al. (1989) data are given in Table 1.

Determination of the iron sulfide composition

During the course of the experiment, the Fe-S monitor changes its composition by losing or gaining sulfur, depending on the sulfur fugacity prevailing during the experiment. The sulfur mole fraction in the Fe-S monitor after the experiment is a function of the sulfur fugacity (see below for more details). In general, an iron sulfide phase at higher temperature cannot be quenched into a single phase due to immiscibility between the Fe-rich component and Fe-S and characteristic S-rich sulfide exsolution lamellae formed during quench. No representative bulk analyses of the iron sulfide can be easily obtained by microanalytical techniques, such as electron microprobe.

If the initial composition and mass of the Fe-S monitor is known, the observed mass gain or loss of the sample is a convenient way to determine the final sulfide composition (weighing method). This method is not the most reliable one because sample recovery may not be complete or sulfur particles, deposited during the experiments at the cool top of the furnace, might adhere to the outside of the container from accidental contact when withdrawing the charge from the furnace. This may introduce errors in the determination of the final mass and hence composition of the Fe-S monitor.

More reliable and less troublesome is the analyses of sulfur in iron sulfide by classical combustion. This method can be applied to an aliquot of the monitor sample, but the Fe-S monitor sample has to be well homogenized by grinding after the experiment. Classical combustion utilizes the mass change associated with the complete oxidation of iron sulfide ($Fe_{1-x}S$) to hematite (Fe_2O_3) and gaseous SO_2 in air at elevated temperatures:

$$2\ Fe_{1-x}S + [2+1.5\cdot(1-x)]\ O_2\ (air) = (1-x)\ Fe_2O_3 + 2\ SO_2\ (g) \qquad [1]$$

The mass change between the initial mass of the $Fe_{1-x}S$ (M_{ini}) aliquot and the final mass of the Fe_2O_3 (M_{fin}) associated with reaction [1] is used to obtain the mole fraction of sulfur of the iron sulfide monitor after the experiment (we define the mole fraction of sulfur, X_S, so that $X_{Fe} + X_S = 1$).

The analytical procedure for the Fe-S monitor after the experiment is as follows. A known mass of the Fe-S monitor sample (M_{ini} = 5 - 120 mg total) was transferred into a small corundum crucible (length 5 mm, ID 6 mm). Up to 10 crucibles with Fe-S monitor samples from different experiments were placed in a muffle furnace at room temperature. The temperature was increased to 250°C over a period of 3 hours in air. After keeping the temperature constant for 2-3 days, the temperature was raised to 500°C within 3 hours and kept constant again for 1 day. After that the temperature was increased to 750°C for at least 1 week and up to three months. The crucibles were then placed directly into a drying oven at 115°C overnight. The crucibles were weighed immediately after taking

them out of the drying oven. Weighing precision was better than ±0.008 mg. Randomly chosen samples were then checked by X-ray diffraction to ensure that combustion is complete and that no magnetite (Fe_3O_4) is present. In all cases, only hematite was found in the combusted samples.

The mole fraction of sulfur (X_S) of the iron sulfide monitor is calculated from the initial and final weight (M_{ini}, M_{fin}) of the sample by

$$X_S = \frac{\frac{M_{ini}}{32.066} - 0.02182 \cdot M_{fin}}{\frac{M_{ini}}{32.066} - 0.00929 \cdot M_{fin}} \quad [2]$$

Depending on the amount of material available for combustion (M_{ini}), this method gives very accurate and precise determinations of the Fe/S ratio in an iron sulfide. Condit et al. (1974) used this method for pyrrhotite analysis and found that Fe/S ratios could be determined to ±0.2%. Fegley et al. (1995) used this method for pyrite analysis and found that Fe/S ratios could be determined to ±0.02%. The results for the X_S determinations from the weighing and combustion methods are given in Table 1. Errors of Fe/S ratios based on precision of multiple weighing of the samples are ±0.0003%.

CONCEPT OF THE FE-S MONITOR METHOD AND CALIBRATION

During the experiment, the Fe-S monitor changes its stoichiometry by either losing or gaining sulfur, depending on its initial composition and superimposed sulfur fugacity according to the reaction

$$FeS_z^{initial} \pm {}^{y}/_{2}\, S_2\,(g) = FeS_{z\pm y}^{final} \quad [3]$$

where $FeS_z^{initial}$ and $FeS_{z\pm y}^{final}$ describe the iron sulfide stoichiometry before and after the experiment and S_2 is the equilibrium sulfur concentration in the gas mixture.

In the following we express the composition by the mole fraction of sulfur X_S, defined as $X_S=N_S/(N_{Fe}+N_S)$, where N is the number of moles of sulfur (N_S) or iron (N_{Fe}) in the bulk iron sulfide phase.

Figure 1A shows the phase relationships as a function of temperature in an "inverted" Fe-S phase diagram, which we use to track the phase assemblages.

EQUATIONS RELATING IRON SULFIDE COMPOSITION TO SULFUR FUGACITY

The Fe-S phase diagram has been extensively investigated and several measurements of the Fe-S stoichiometry as a function of sulfur fugacity or sulfur activity at high temperatures are available (e.g., Bale and Toguri 1976; Bog and Rosenqvist 1958; Burgmann et al. 1968 ; Ditman and Vecko 1965; Nagamori and Kameda 1965; Nagamori et al. 1970; Štofko et al. 1974). The thermodynamic derivation of the sulfur fugacity as a function of sulfide composition is quite complex (e.g., Schürmann and Henke (1972); Sharma and Chang (1979); Guillermet et al. (1981); Chuang et al. (1985); Kress (2007) and references therein). It is generally difficult to model defect-structure thermodynamics, which becomes important at the S-poor side of the Fe-S phase diagram ($X_S<0.5$). Sharma and Chang (1979) and Kress (1997) describe two somewhat different approaches to thermodynamically derive the Fe-S phase diagram and the sulfur fugacities as a function of the sulfur mole fraction. Their mathematical procedures are lengthy and impractical for our purposes, because we are interested in a convenient method relating sulfide composition to sulfur fugacity. Thus, we want to develop a practical relationship between the sulfur mole fraction in the bulk system and the sulfur fugacity.

225

226 **Sulfur fugacity over Fe-S melts saturated with solid iron**

227 We begin our description of the sulfur fugacities at the iron-rich side of the Fe-S phase diagram,
228 where Fe-S melts are saturated with solid iron. Metal and sulfide liquid are immiscible above the
229 eutectic temperature (988°C) and have lower mole fractions of sulfur than present at the eutectic
230 (X_S=0.446). The minimum X_S for coexisting iron-rich sulfide liquid and Fe-metal as a function of
231 temperature is shown in Figure 1A. In Figure 1B, we plot literature data for sulfur fugacities at 1000
232 - 1400°C (Bale and Toguri 1976; Bog and Rosenqvist 1958; Nagamori et al. 1970; Sharma and
233 Chang 1979; Chuang et al. 1985; Rosenqvist and Dunicz 1952; Rosenqvist 1954). We approximate
234 the sulfur fugacities over γ-iron-saturated melts for 1000-1365°C by

235 $$\log fS_2 = 18.840(\pm 4.494) - 23276(\pm 3188)\ T(K) - 0.00578(\pm 0.00158)/T(K) \quad [4]$$

236 The log fS_2 is plotted versus temperature in degree Celsius in Figure 1B for convenience but note
237 that equation [4] uses T in Kelvin. The calculated curve in Figure 1B includes all experimental data
238 for γ-iron-saturated melts except the three points by Nagamori et al. (1970) that are consistently
239 higher by 0.21 to 0.36 log-units than the sulfur fugacities observed in other studies.
240 The sulfur fugacity can be derived from Figure 1A and equation [4] if the Fe-S monitor after the
241 experiment has a bulk composition that corresponds to an equilibrium assemblage of Fe-S melt plus
242 solid γ-Fe at run temperature. For example, at 1300°C, an Fe-S monitor composition of $X_S \leq 0.325$
243 indicates iron saturation and the equilibrium sulfur partial pressure from equation [4] gives log fS_2 =
244 -5.05. Equation [4] should not be extrapolated beyond the high temperature limit of 1365°C. The
245 high temperature limit of equation [4] is given by the appearance of δ-metallic iron and the sulfur

246 solubility in δ-metallic iron at very low X_S (see Rosenqvist and Dunicz (1952) and Ban-ya and
247 Chipman (1968) for sulfur solubility in solid iron).

248 At a given temperature and as long as the iron sulfide melt is saturated with solid iron, a three
249 phase equilibrium with Fe solid + Fe-S melt + S_2 gas exists, so that the sulfur fugacity is fixed. The
250 iron sulfide melt always has the same composition at that given temperature. In the bulk system
251 consisting of iron sulfide melt plus solid iron, the overall X_S in the system can vary at that given
252 temperature. The absolute amounts of iron sulfide melt plus solid iron are irrelevant as long as these
253 phases are present because the fS_2 remains constant, since the activities of the iron sulfide melt and
254 solid iron remain unity. Equation [4] can therefore be used to calculate the sulfur fugacity at any
255 given temperature between 1000-1365°C when iron saturated Fe-S liquid was present at
256 experimental temperatures.

257 We also remind the reader that the sulfur fugacities over iron saturated Fe-S melts do not
258 correspond to the equilibrium of solid iron and stoichiometric FeS melts for which thermodynamic
259 properties are listed in many compilations such as the JANAF Tables (Chase 1998). The phase
260 diagram in Figure 1A shows that the composition of the Fe-S melt coexisting with solid iron varies
261 with temperature. The sulfur fugacities for the hypothetical equilibrium of solid iron with
262 stoichiometric FeS melt from the thermochemical equilibrium data in Chase (1998) are shown by the
263 dashed line in Figure 1B for comparison.

264

265 **Sulfur fugacity over Fe-S melts**

266 Our experimental data and literature values for the sulfur fugacity as a function of the sulfur mole
267 fraction from 1100°C to 1400°C are plotted in Figure 2. The data range from iron saturated melts to
268 sulfur-rich compositions up to X_S of about 0.53. The literature sources are given in the Figure

caption and are distinguished by different symbols. Solid dots show our experimental data listed in Table 1. The sulfur fugacity at iron saturation obtained from equation [4] is shown by a cross for each temperature.

The vertical lines in the diagrams show the phase boundaries from the phase diagram (Kubaschewski 1982) and the stable phases are indicated. The most complex case shown is for 1100°C. This is the only temperature considered where Fe-S melts coexist with γ-$Fe_{1-x}S$ solid, or only γ-$Fe_{1-x}S$ solid is present at larger X_S. At the higher temperatures, we only have to consider Fe-S melts and iron saturated Fe-S melts. The sulfur fugacities over the iron saturated Fe-S melts are already described above and equation [4] can be used to calculate their sulfur fugacities.

The dotted lines drawn through the data in Figure 2 are our derived functions for the sulfur fugacity dependence on the mole fraction of sulfur. We used a simple thermodynamic approach to derive our functions for the sulfur fugacities over Fe-S melts (Table 2).

For this approach we assume that the S_2 fugacity over a Fe-S melt is controlled by the reaction

$$2\ S_{liq} = S_2\ (gas) \qquad [5]$$

that relates fS_2 to the activity of liquid sulfur in the Fe-S melt. As neither the S_2 fugacity nor the activity of liquid sulfur in the Fe-S melt are unity, varying S_2 fugacity will result in varying Fe/S ratios of the Fe-S melt.

The equilibrium constant for reaction [5] is $K = fS_2 / (a_{liq})^2$. Substituting the activity of liquid sulfur by the sulfur mole fraction and its activity coefficient (γ_S), and rearranging yields the logarithmic form for the sulfur fugacity as

$$\log fS_2 = \log K + 2 \log X_S + 2 \log \gamma_S \qquad [6]$$

290 The activity coefficient γ_S is defined by the excess Gibbs energy (g^E/RT) and its differential towards
291 X_S and can be expressed as

292 $$\ln \gamma_S = g^E/RT + [1-X_S]\, d(g^E/RT)/dX_S \quad [7]$$

293 The Redlich-Kister equation (Redlich and Kister 1948) for the excess Gibbs energy as a function of
294 liquid composition is

295 $$g^E/RT = X_1 X_2 [c_1 + c_2 (X_1 - X_2) + c_3 (X_1 - X_2)^2 + \ldots] \quad [8]$$

296 The Redlich-Kister equation fulfills the requirement that g^E is zero at $X_S = 0$ and at $X_S = 1$.
297 We find that an expansion to include the quadratic term is sufficient to satisfactorily fit the data and
298 is used in the following.
299 Replacing g^E/RT and its differential in equation [7] by the Redlich-Kister equation [8] and its
300 differential, respectively, and further rearranging yields

301 $$\ln \gamma_S = (1-X_S)^2 [\, A + 2\, B\, (1-X_S) + 3\, C\, (1-X_S)^2] \quad [9]$$

302 Here c_1, c_2, and c_3 of equation [8] are parameters for the excess Gibbs energy, and the parameters A,
303 B, and C of equation [9] are algebraic combinations thereof, e.g., $A = c_1 - 3\, c_2 - 19\, c_3$, $B = 2\, c_2 + 16$
304 c_3, $C = -4\, c_3$.

305 We substitute equation [9] into equation [6] and fit the sulfur fugacities as

306 $$\log fS_2 = d + 2 \log X_S + 2\, (1-X_S)^2 [\, a + 2\, b\, (1-X_S) + 3\, c\, (1-X_S)^2] \quad [10]$$

307 The equations for log fS_2 over Fe-S melts as functions of X_S for the four temperatures are listed in
308 Table 2. The sulfur fugacities over iron-saturated melts (horizontal lines at the lowest X_S in Figure 2)

are from equation [4]. The fits for the non-saturated and saturated Fe-S melt, and solid fields for 1100°C use simple polynomial fits (also listed in Table 2) because they span only small ranges for X_S. Ideally, we would use all data to find a fit that simultaneously describes log fS_2 as a function of X_S and temperature. We tested whether a reliable fit could be obtained but only found solutions that are plagued with high uncertainties in the fit parameters. More data would be needed to produce a reasonable fit from which interpolations in temperature for log fS_2 can be made confidently.

At 1200°C, the data by Nagamori et al. (1970, shown as triangles) plot at higher fS_2 than the data by Bale and Toguri (1976, shown as squares) for $X_S < 0.5$. Closer to $X_S = 0.5$, they are lower than those by Bale and Toguri (1976), and lower than those by Burgmann et al. (1968, shown as circles). With only two studies covering $X_S<0.5$, it is not easily clear which study is off. However, the sulfur fugacities derived by Nagamori et al. (1970) were also consistently higher than those from other studies for iron-saturated melts compared in Figure 1B. The reason for the discrepancies of the data by Nagamori et al. (1970) cannot be the use of H_2-H_2S gas mixtures here instead of CO-CO_2-SO_2 gas mixtures. Other literature studies also use H_2-H_2S gas mixtures and where a comparison is possible, the Nagamori et al. (1970) data seem to be off the trends indicated by other literature studies (see Figure 1B and Figure 2, especially for 1200°C). Another example that let us to believe that the data by Nagamori et al. (1970) are more uncertain is that the sulfur fugacity at 1300°C by Nagamori et al. (1970) coincides with that of Bog and Rosenqvist (1958) at 1400°C for the same X_S of about 0.415 although the temperatures are different. The experimental literature studies show somewhat inconsistent results and there is no consensus of which experimental set is more reliable. For example, Guillermet et al. (1981) and Chuang et al. (1985) conclude that the data by Bog and Rosenqvist (1958) are uncertain, while Štofko et al. (1974) regard the data by Nagamori et al. (1970) as less reliable. Overall, the data by Nagamori et al. (1970) show the largest deviation from the other

data sets where a direct comparison can be made and we did not include their data in the fits for 1200°C and 1300°C. The fit results for 1200°C for the selected literature data are in Table 2.

The exclusion of the Nagamori et al. (1970) data makes it difficult to obtain a reliable fit at 1300°C for the entire range of X_S where Fe-S melt is present. We only have the data from Burgmann et al. (1968) and Ditman and Vecko (1965) for $X_S > 0.488$ (open circles and diamonds in Figure 2 - 1300°C). In order to derive a fit for 1300°C for the entire range down to $X_S = 0.325$, where the melt becomes saturated in Fe, we decided to combine our experimental results with the literature data. We are aware of the fact that at higher X_S the Nagamori et al. (1970) data and our data overlap, but at X_S values close to iron saturated Fe-S melts the Nagamori et al. (1970) data are too high, as already shown in Figure 1B.

There are no data from Nagamori et al. (1970) for 1400°C, and we used the data from Bog and Rosenqvist (1958) and Ditman and Vecko (1965) for the fit. There are only two data points at 1400°C for $0.125 < X_S < 0.38$, which are both for iron-saturated melts (namely, the point for X_S at iron saturation and the value for $X_S = 0.38$). In lieu of other data, we made a linear approximation for the range $0.125 < X_S < 0.38$. For the non-saturated Fe-S melt, we fit the data of XS =0.38 and above.

Please note that the motivation of our study was to provide a method to utilize the stoichiometry of iron sulfide to determine the sulfur fugacity in experiments containing CO-CO_2-SO_2 gas mixtures. We derived equations with literature data and tested them by our own experimental data. We did not use our experimental data as input data to the parameterization, except for 1300°C (see above). The fits to the literature data at 1200°C and 1400°C generally reproduce our experimental log fS_2 within 0.15 log units and better. Other more complex thermodynamic derivations of the sulfur fugacity by, e.g., Sharma and Chang (1979), Guillermet et al. (1981), Chuang et al. (1985), Kress (2007), Kress (1997) and references therein have similar uncertainties.

355

356 **COMPARISON OF VARIOUS METHODS TO DETERMINE OXYGEN AND SULFUR FUGACITIES**

357 Before we compare the different ways to determine the sulfur fugacity in our experiments we
358 compare the results of the different methods to determine the oxygen fugacities.

359

360 **Oxygen fugacity determinations**

361 **fO_2 computed from thermodynamic data.**

362 The fO_2-values prevailing in the experiments calculated from the two thermodynamic data sets of
363 Chase et al. (1998) and Gurvich et al. (1989) and the composition of the initial CO-CO_2-SO_2 gas
364 mixtures are given in Table 1 and plotted in Figure 3A. The solid line indicates the ideal 1:1
365 correlation and the dotted lines are the 1 % deviations relative to the 1:1 line. Both sets of fO_2-values
366 agree well and their deviation is significantly less than 1%. The log fO_2 calculated with the
367 thermodynamic data set of Chase et al. (1998) is typically 0.04 log units more negative, which
368 means that the fO_2 from Chase et al. (1998) is about a factor of 0.91 smaller than that of Gurvich et
369 al. (1989).

370

371 **fO_2 determination by solid electrolyte sensor.**

372 The fO_2 values directly measured with CaO-Y_2O_3-doped ZrO_2 solid electrolyte sensors are given
373 in Table 1. Oxygen fugacities measured with solid electrolyte sensors and calculated fO_2-values by
374 using the two thermodynamic data sets are plotted in Figures 3B and 3C. The solid line indicates the
375 ideal 1:1 correlation. The dotted lines are 5 % deviations relative to the 1:1 correlation. The
376 deviation between calculated fO_2-values by using data of Chase et al. (1998), Gurvich et al. (1989),

and the measured in-situ fO_2-values is in most cases within 2 %. All fO_2-values plot within the field of 5 % deviation.

Sulfur fugacity determinations

fS_2 computed from thermodynamic data.

The sulfur fugacity values prevailing in the experiments are calculated from thermodynamic data and the composition of the initial CO-CO_2-SO_2 gas mixtures by using thermodynamic data from Gurvich et al. (1989) as well as Chase et al. (1998), where we included corrected data from Lodders (2004). The values are given in Table 1 and plotted in Figure 4A. The solid line shows the 1:1 correlation. The dotted lines are 5 % deviations relative to the 1:1 correlation. The individual deviations are less than 3 %. The agreement of both sets of fS_2-values is good but not as good as for the calculated fO_2-values mentioned above. The deviation of the sulfur fugacity values calculated with the thermodynamic data set of Chase et al. (1998) compared to the values calculated with the thermodynamic data set of Gurvich et al. (1989) is the opposite to the deviation of both sets of oxygen fugacities: the data of Chase et al. (1998) are on average 0.15 (1200°C), 0.11 (1300°C), and 0.07 (1400°C) log-units lower than those of Gurvich et al. (1989), so the sulfur fugacities of Chase et al. (1998) are factors of about 1.4 (1200°C), 1.3 (1300°C), and 1.2 (1400°C) larger than those from the Gurvich data set.

fS_2 determination by solid electrolyte sensor.

Due to the lack of available solid electrolyte sensors to determine sulfur fugacities at experimental run temperatures above 1000°C, fS_2 could not be directly measured during the experiments.

400 **fS_2 determination from the stoichiometry of iron sulfide monitors.**

401 The results for the different ways of determining the sulfur mole fraction, i.e., weighing method
402 and combustion, are compared in Table 1 and in Figure 4B. If the sulfur mole fractions determined
403 by both methods agree, they should plot along the ideal 1:1 correlation line (shown as solid line in
404 Figure 4B). We find that the methods agree within 5 % (dotted black line), except for S-poor iron
405 sulfides and small aliquot masses. The exceptions are indicated in the Figure by numbers which
406 correspond to the following samples, which all yield a lower X_S from the weighing method than the
407 combustion method: #1: S-I-16, #2: S-I-18, #3: S-II-8, #4: S-I-11, #5: S-IV-16. Even for these
408 outliers sulfur mole fractions determined by weighing method and combustion agree still within 15
409 % (dotted grey line). In general, the determination of sulfur in small samples by the weighing
410 method (< 30 mg total sample mass) and by the combustion method (≤ 10 mg, aliquot used for
411 combustion) seems to become less reliable and thus the calculation of the sulfur mole fraction
412 becomes more uncertain. For good measurements, at least 50-75 mg of Fe-S monitor is needed.
413 Figure 4C compares sulfur fugacities for each individual experiment at 1200°C and 1400°C
414 calculated for the inlet gas mixture composition using thermodynamic data by Chase et al. (1998),
415 "log fS_2 (Chase)", with the sulfur fugacities calculated from equation [10] and fit coefficients in
416 Table 2, "log fS_2 (fit)". The sulfur mole fractions needed to calculate log fS_2 from equation [10] are
417 obtained from the combustion method. Only data at 1200°C and 1400°C are compared in Figure 4C
418 (Note that the fit for 1300°C (from, equation [10], see Table 2) does include our experimental
419 results). At 1400°C the deviation of both sulfur fugacities, i.e., log fS_2 (Chase) and log fS_2 (fit), is
420 well below 10 % (black dotted line). At 1200°C, the lower sulfur fugacities also agree within 10 %,
421 but the deviation is about 15 % at higher sulfur fugacities (grey dotted line).
422

CONCLUSIONS

We present a method to determine the sulfur fugacity in experiments containing CO-CO_2-SO_2 gas mixtures at ambient pressures by placing iron sulfide as monitor next or close to the experimental charge. During the experiment, the Fe-S monitor changes its stoichiometry through losing or gaining sulfur, depending on the sulfur fugacity in the gas mixture. Relations for the sulfur fugacity as function of mole fraction of sulfur (X_S) in the Fe-S monitor after the experiments are derived for temperatures of 1100°C, 1200°C, and 1400°C from experimental data in the literature, and for 1300°C from experimental data in the literature and our data. We used the Redlich-Kister approach to derive an equation to relate the fS_2 to X_S for sulfur-rich Fe-S melts and compared it to results from our Fe-S monitor experiments at 1200°C and 1400°C. The sulfur fugacity derived from the Fe-S monitor agrees with the sulfur fugacity calculated for the CO-CO_2-SO_2 gas mixtures from the thermodynamic data of the coexisting gaseous compounds in most of the experiments within 0.15 log units. The Fe-S monitor method allows an independent check of the sulfur fugacity prevailing in experiments containing CO-CO_2-SO_2 gas mixtures as long as oxygen fugacities remain below that of the iron-wüstite or iron-magnetite buffer.

ACKNOWLEDGMENTS

The experiments were carried out during multiple visits of A. Holzheid at the Planetary Chemistry Laboratory at Washington University in St. Louis. We thank Bruce Fegley for advice and fruitful discussions. We thank D. Kremser, formerly Washington University, St. Louis, for help and assistance in analyzing the samples by X-ray diffraction technique. Comments by an anonymous referee and Alexander Borisov are appreciated. Financial support was provided through the German Academic Exchange Service (DAAD) and the German Science Foundation (DFG) to one of us

446 (AH). We also thank the McDonnell Center for the Space Science to provide housing support for
447 AH during her visits to Washington University.

448

REFERENCES

Bale, C.W. and Toguri, J.M. (1976) Thermodynamics of the Cu-S, Fe-S and Cu-Fe-S systems. Canadian Metallurgical Quarterly, 15-4, 305-318.

Ban-ya, S. and Chipman, J. (1968) Sulfur in liquid iron alloys I. Binary Fe-S. Transactions of the Metallurgical Society of AIME, 242, 940-946.

Bezmen, N.I., Asif, M., Brügmann, G.E., Romanenko, I.M., and Naldrett, A.J. (1994) Distribution of Pd, Rh, Ru, Ir, Os, and Au between sulfide and silicate melts. Geochimica et Cosmochimica Acta, 58, 1251-1260.

Bog, S. and Rosenqvist, T. (1958) Thermodynamics of metal sulphides: I: A thermodynamic study of the iron sulphide - iron oxide melts. Communication Metallurgical Research, 12, 6 B.

Bouhifd, M.A. and Jephcoat, A.P. (2011) Convergence of Ni and Co metal–silicate partition coefficients in the deep magma–ocean and coupled silicon–oxygen solubility in iron melts at high pressures. Earth and Planetary Science Letters, 307, 341–348.

Burgmann, W., Urbain, G., and Frohberg, M.G. (1968) Contribution à l'étude du système fer-soufre limité au domaine du mono-sulfure de fer (pyrrhotine). Memoires Scientifiques de la Revue de Metallurgie, 65 7/8, 567-578.

Chabot, N.L. and Jones, J.H. (2003) The parameterization of solid metal-liquid metal partitioning of siderophile elements. Meteoritics and Planetary Sciences, 38, 1425-1436.

Chabot, N.L., Campbell, A.J., Jones, J.H., Humayun, M., and Agee, C.B. (2003) An experimental test of Henry's Law in solid metal-liquid metal systems with implications for iron meteorites. Meteoritics and Planetary Sciences, 38, 181-196.

Chase, M.W. (1998) NIST-JANAF Thermochemical Tables, 4th ed., Journal of Physical and Chemical Reference Data, Monograph 9, American Institute of Physics, 1951 p. Woodbury, New York.

Chuang, Y.Y., Hsieh, K.C., and Chang, Y.A. (1985) Thermodynamics and phase relationships of transition metal-sulfur systems: Part IV. A reevaluation of the Fe-S system using an associated solution model for the liquid phase. Metallurgical Transactions, B 16, 277-285.

Condit, R.H., Hobbins, R.R., and Birchenall, C.E. (1974) Self-diffusion of iron and sulfur in ferrous sulfide. Oxidation of metals, 8, 409-455.

Corgne, A., Keshav, S., Wood, B.J., McDonough, W.F., and Fei, Y. (2008) Metal–silicate partitioning and constraints on core composition and oxygen fugacity during Earth accretion. Geochimica et Cosmochimica Acta, 72, 574–589.

Cottrell, E., Walter, M.J., and Walker, D. (2009) Metal-silicate partitioning of tungsten at high pressure and temperature: Implications for equilibrium core formation in Earth. Earth and Planetary Science Letters, 281, 275–287.

Cottrell, E., Walter, M.J., and Walker D. (2010) Erratum to Metal-silicate partitioning of tungsten at high pressure and temperature: Implications for equilibrium core formation in Earth (vol 281, pg 275, 2009). Earth and Planetary Science Letters, 289, 631–634.

Ditman, A.V. and Vecko, I.N. (1965) High-temperature iron sulfide dissociation studied by the dew point method. Neorganicheskie materialy (Inorganic materials), 1, 1530-1536 (in Russian).

Fegley, B. (2013) Practical chemical thermodynamics for geoscientists, 674 p. Academic Press - Elsevier, Waltham.

Fegley, B., Lodders, K., Treiman, A.H., and Klingenhöfer, G. (1995) The rate of pyrite de-composition on the surface of Venus. Icarus, 115, 159-180.

493 Gauthier, M., Chamberland, A., Bélanger, A., and Poirier, M. (1977) Solid-state detectors for the
494 potentiometric determination of gaseous oxides II. Measurements in oxygen-variable gases in
495 the SO_2, SO_3, O_2, Pt/SO_4-system. Journal of the Electrochemical Society, 124-10, 1584-1587.
496 Guillermet, A.F., Hillert, M., Jansson, B., and Sundman, B. (1981) An assessment of the Fe-S
497 system using a two-sublattice model for the liquid phase. Metallurgical Transactions, B 12,
498 745-754.
499 Gurvich, L.V., Veyts, I.V., and Alcock, C.B. (1989) Thermodynamic properties of individual
500 substances, Vol. 1-4, 4th ed., 2322 p. Hemisphere Publ., New York.
501 Holzheid, A. and Lodders, K. (2001) Solubility of copper in silicate melts as function of oxygen and
502 sulfur fugacity, temperature, and silicate composition. Geochimica et Cosmochimica Acta, 65,
503 1933-1951.
504 Holzheid, A. and Palme, H. (2007) The formation of eucrites: Constraints from metal-silicate
505 partition coefficients. Meteoritics and Planetary Science, 42, 1817–1829.
506 Kegler, P. and Holzheid, A. (2011) Determination of the formal Ge-oxide species in silicate melts at
507 oxygen fugacities applicable to terrestrial core formation scenarios. European Journal of
508 Mineralogy, 23, 369-378.
509 Kegler, P., Holzheid, A., Frost, D.J., Rubie, D.C., Dohmen, R., and Palme, H. (2008) New Ni and
510 Co metal-silicate partitioning data and their relevance for an early terrestrial magma ocean.
511 Earth and Planetary Science Letters, 268, 28–40.
512 Kress, V. (1997) Thermochemistry of sulfide liquids I: The system O-S-Fe at 1 bar. Contributions to
513 Mineralogy and Petrology, 127, 176-186.
514 Kress, V. (2007) Thermochemistry of sulfide liquids III: Ni-bearing liquids at 1 bar. Contributions to
515 Mineralogy and Petrology, 154, 191-204.

516 Kubaschewski, O. (1982) Iron-binary phase diagrams, 185 p. Springer Verlag, Berlin.

517 Li, J. and Agee, C.B. (1996) Geochemistry of mantle-core differentiation at high pressure. Nature,
518 381, 686-689.

519 Lodders, K. (2003) Solar system abundances and condensation temperatures of the elements.
520 Astrophysical Journal, 591, 1220-1247.

521 Lodders, K. (2004) Revised and updated thermochemical properties of the gases mercapto (HS),
522 disulfur monoxide (S2O), thiazyl (NS), and thioxophosphino (PS). Journal of Physical and
523 Chemical Reference Data, 33, 357-367.

524 Lodders, K. and Palme, H. (1991) The role of sulfur in planetary core formation. Meteoritics, 26, A
525 366.

526 Lodders, K. and Fegley, B. (1998) The planetary scientist's companion, 371 p. Oxford University
527 Press, New York.

528 Mann, U., Frost, D.J., and Rubie, D.C. (2009) Evidence for high-pressure core-mantle differentiation
529 from the metal-silicate partitioning of lithophile and weakly siderophile elements. Geochimica
530 et Cosmochimica Acta, 73, 7360–7386.

531 Maruyama, T. (1991) Solid electrolyte sensors for gaseous oxides for pollution monitoring.
532 Materials Science and Engineering A, 146, 81-89.

533 Maruyama, T., Saito, Y., Matsumoto, Y., and Yano, Y. (1985) Potentiometric sensors for sulfur
534 oxides using Nasicon as a solid electrolyte. Solid State Ionics, 17, 281-316.

535 Mungall, J.E. and Naldrett, A.J. (2008) Ore deposits of the Platinum-group elements. Elements, 4,
536 253–258.

537 Nagamori, M. and Kameda, M. (1965) Equilibria between Fe-S-O system melts and CO-CO_2-SO_2
538 gas mixtures at 1200°C. Transactions of the Japan Institute of Metals, 6, 21-30.

539 Nagamori, M., Hatakeyama, T., and Kameda, M. (1970) Thermodynamics of Fe-S melts between
540 1100° and 1300°C. Transactions of the Japan Institute of Metals, 11, 190-194.
541 Palme, H., Kegler, Ph., Holzheid, A., Frost, D.J., and Rubie, D.C. (2011) Comment on „Prediction
542 of metal–silicate partition coefficients for siderophile elements: an update and assessment of PT
543 conditions for metal–silicate equilibrium during accretion of the Earth" by K. Righter, EPSL
544 304 (2011) 158-167, 2011. Earth and Planetary Science Letters, 312, 516–518.
545 Peach, C.L. and Mathez, E.A. (1993) Sulfide melt - silicate melt distribution coefficients for nickel
546 and iron and implications for the distribution of other chalcophile elements. Geochimica et
547 Cosmochimica Acta, 57, 3013-3021.
548 Poulson, S.R. and Ohmoto, H. (1990) An evaluation of the solubility of sulfide sulfur in silicate
549 melts from experimental data and natural samples. Chemical Geology, 85, 57–75.
550 Redlich, O. and Kister, A.T. (1948) Algebraic presentation of thermodynamic properties and the
551 classification of solutions. Industrial and Engineering Chemistry, 40, 345-348.
552 Righter, K. (2003) Metal-silicate partitioning of siderophile elements and core formation in the early
553 Earth. Annual Review of Earth and Planetary Sciences, 31, 135–174.
554 Righter, K. (2011) Prediction of metal–silicate partition coefficients for siderophile elements: an
555 update and assessment of PT conditions for metal–silicate equilibrium during accretion of the
556 Earth. Earth and Planetary Science Letters, 304, 158–167.
557 Rosenqvist, T. (1954) A thermodynamic study of the iron, cobalt and nickel sulphides. Journal of the
558 Iron and Steel Institute, 176, 37-57.
559 Rosenqvist, T. and Dunicz, B.L. (1952) Solid solubility of sulphur in iron. Transactions of the
560 Metallurgical Society of AIME, 194, 604-608.

561 Saito, Y., Maruyama, T., and Yano, Y. (1986) Dissociation pressures of metal sulfates by elec-
562 tromotive force measurement on SO_2-O_2-SO_3 concentration cells with Nasicon solid electrolyte.
563 Canadian Metallurgical Quarterly, 25, 51-57.
564 Schürmann, E. and Henke, H.-J. (1972) Zur Thermodynamik des Systems Eisen-Schwefel.
565 Giessereiforschung, 24/1, 1-9.
566 Sharma, R.C. and Chang, Y.A. (1979) Thermodynamics and phase relationships of transition metal-
567 sulfur systems: Part III. Thermodynamic properties of the Fe-S liquid phase and the
568 calculations of the Fe-S phase diagram. Metallurgical Transactions, B 10, 103-108.
569 Siebert, J., Badro, J., Antonangeli, D., and Ryerson, F.J. (2012) Metal–silicate partitioning of Ni and
570 Co in a deep magma ocean. Earth and Planetary Science Letters, 321-322, 189–197.
571 Siebert, J., Corgne, A., and Ryerson, F.J. (2011) Systematics of metal–silicate partitioning for many
572 siderophile elements applied to Earth's core formation. Geochimica et Cosmochimica Acta, 75,
573 1451-1489.
574 Štofko, M., Schmiedl, J., and Rosenqvist, T. (1974) Thermodynamic of iron-sulphur-oxygen melts at
575 1200°C. Scandinavian Journal of Metallurgy, 3, 113-118.
576 Walter, M.J., Newsom, H.E., Ertel, W., and Holzheid A. (2000) Siderophile elements in the Earth
577 and Moon: metal-silicate partitioning and implications for core formation. In: R. Canup and K.
578 Righter, Eds., Origin of the Earth and Moon, p. 235-289. University of Arizona Press, Tuscon,
579 Arizona.
580

TABLE 1. Experimental run parameters, calculated and measured oxygen fugacities, calculated sulfur fugacities, and mole fractions of sulfide in Fe-S monitor determined by mass difference and combustion (in order of temperature and X_S)

run	T [°C]	Duration [h]	CO-CO_2-SO_2 *	log fO_2 †	log fO_2 ‡	log fO_2 §	log fS_2 ‖	log fS_2 #	X_S **	X_S ††
1200°C										
S-III-21 ‡‡	1205	73	91.97-5.03-3.00	-12.82	-12.77	-12.20	-5.04	-5.22	0.451	0.450
S-III-10 ‡‡	1200	69.1	91.96-8.00-0.04	-12.92	-12.88	N/A §§	-4.62	-4.79	0.471	0.469
S-III-13 ‡‡	1201	65.6	91.95-8.00-0.05	-12.93	-12.88	N/A §§	-4.05	-4.20	0.484	0.483
S-III-14 ‡‡	1203	65.6	91.92-7.99-0.08	-12.61	-12.56	-12.61	-3.65	-3.79	0.473	0.485
S-III-16 ‡‡	1202	53.4	91.86-7.99-0.15	-12.79	-12.75	N/A §§	-3.36	-3.48	0.482	0.492
S-III-19 ‡‡	1200	70.3	91.86-7.99-0.15	-12.87	-12.83	-12.91	-3.70	-3.83	0.496	0.495
1300°C										
S-I-16 ‡‡	1300	72.5	88.76-11.21-0.03	-11.54	-11.50	-11.72	-5.08	-5.24	0.344	0.381
S-I-18 ‡‡	1300	71	87.19-12.78-0.03	-11.40	-11.36	-11.72	-4.98	-5.13	0.333	0.394
S-II-9 ‡‡	1303	68.5	95.27-4.68-0.05	-12.31	-12.27	-12.47	-4.61	-4.76	0.419	0.417
S-II-6 ‡‡	1299	72.0	93.12-6.81-0.07	-12.00	-11.96	-12.09	-4.31	-4.45	0.416	0.417
S-II-7 ‡‡	1300	30.5	93.01-6.92-0.07	-11.98	-11.94	-12.18	-4.29	-4.43	0.413	0.417
S-III-5 ‡‡	1301	40.9	91.98-8.00-0.02	-11.56	-11.52	-11.69	-4.83	-4.99	0.428	0.426
S-II-8 ‡‡	1304	42.0	94.11-5.84-0.06	-12.09	-12.05	-12.63	-4.43	-4.57	0.370	0.427
S-I-15 ‡‡	1300	55	88.65-11.26-0.09	-11.52	-11.48	-11.82	-4.08	-4.21	0.432	0.435
S-I-17 ‡‡	1301	72	92.25-7.68-0.06	-11.87	-11.83	-11.72	-4.37	-4.51	0.422	0.437
S-I-17 ‖‖	1301	72	92.25-7.68-0.06	-11.87	-11.83	-11.72	-4.37	-4.51	0.442	0.444
S-III-12 ‡‡	1299	65.6	91.87-7.99-0.14	-12.09	-12.06	-12.32	-4.58	-4.73	0.452	0.441
S-I-14 ‡‡	1301	65.5	91.50-8.44-0.06	-11.94	-11.90	-11.74	-4.43	-4.57	0.434	0.444
S-I-11 ‡‡	1302	44	92.69-7.01-0.30	-11.88	-11.84	-11.78	-3.27	-3.36	0.377	0.452
S-IV-6 ‡‡	1300	73.1	90.44-9.44-0.12	-11.67	-11.63	-11.75	-3.88	-4.01	0.460	0.456
S-III-4 ‡‡	1299	43.2	91.95-8.00-0.05	-11.75	-11.71	N/A §§	-4.37	-4.51	0.455	0.459
S-I-11 ‖‖	1302	44	92.69-7.01-0.30	-11.88	-11.84	-11.78	-3.27	-3.36	0.461	0.462
S-IV-3 ‡‡	1302	74.5	92.37-7.44-0.19	-11.85	-11.81	-11.61	-3.57	-3.68	0.474	0.464
S-III-6 ‡‡	1300	69.6	91.54-7.96-0.50	-12.28	-12.24	-12.02	-3.09	-3.17	0.464	0.468
S-III-6-2 ‡‡	1300	69.6	91.54-7.96-0.50	-12.28	-12.24	-12.02	-3.09	-3.17	0.467	0.469
S-IV-12 ‡‡	1302	48.1	90.00-9.50-0.50	-11.57	-11.52	-11.69	-2.95	-3.02	0.476	0.475
S-IV-1 ‡‡	1301	94.3	90.00-9.50-0.50	-11.58	-11.54	-11.72	-2.95	-3.02	0.470	0.476

S-IV-15 ‡‡	1301	23.9	90.00-9.50-0.50	-11.58	-11.54	-11.64	-2.95	-3.02	0.473	0.476
S-IV-9 ‡‡	1301	71.2	90.00-9.50-0.50	-11.58	-11.54	-11.70	-2.95	-3.02	0.480	0.477
S-I-12 ‡‡	1300	51.5	92.08-4.30-3.62	-11.47	-11.43	-11.78	-1.87	-1.90	0.494	0.501
S-I-12 ||||	1300	51.5	92.08-4.30-3.62	-11.47	-11.43	-11.78	-1.87	-1.90	0.506	0.508
1400°C										
S-IV-11 ‡‡	1399	71.0	98.25-1.66-0.09	-12.08	-12.05	-11.69	-3.92	-4.03	0.415	0.427
S-IV-5 ‡‡	1398	73.7	97.50-2.38-0.13	-11.77	-11.74	-11.57	-3.68	-3.77	0.429	0.446
S-IV-10 ‡‡	1398	71.2	94.35-5.52-0.13	-11.06	-11.03	-10.85	-3.66	-3.75	0.443	0.451
S-IV-8 ‡‡	1399	72.7	96.91-2.94-0.15	-11.58	-11.54	-11.25	-3.58	-3.66	0.452	0.451
S-IV-4 ‡‡	1399	74.1	95.16-4.60-0.24	-11.17	-11.14	-11.09	-3.28	-3.35	0.457	0.460
S-IV-7 ‡‡	1400	72.9	90.87-9.01-0.12	-10.60	-10.57	-10.36	-3.70	-3.79	0.441	0.462
S-IV-14 ‡‡	1400	48.0	90.00-9.50-0.50	-10.48	-10.44	-10.31	-2.84	-2.89	0.466	0.464
S-IV-13 ‡‡	1398	72.2	90.00-9.50-0.50	-10.50	-10.46	-10.41	-2.84	-2.89	0.467	0.469
S-IV-2 ‡‡	1399	94.2	90.00-9.50-0.50	-10.49	-10.45	-10.43	-2.84	-2.89	0.464	0.470
S-IV-16 ‡‡	1400	23.9	90.00-9.50-0.50	-10.48	-10.44	-10.31	-2.84	-2.89	0.457	0.506

585
586 $CO-CO_2-SO_2$ gas mixture in %; † calculated log fO_2 using data from Chase (1998); ‡ calculated log fO_2 using data from
587 Gurvich et al. (1989); § measured log fO_2 with solid state electrolyte sensors; || calculated log fS_2 using data from Chase (1998);
588 ¶ calculated log fS_2 using data from Gurvich et al. (1989); ** X_S determined by direct differences in mass before and after the
589 experiment; †† X_S determined gravimetrically by combustion (and plotted in Figure 2); ‡‡ commercial FeS used as Fe-S
590 monitor; §§ no solid state electrolyte sensor was in the furnace, measured log fO_2 value does not exist; |||| synthetic FeS used as
591 Fe-S monitor. Please note: Errors of X_S determinations due to precision of multiple weighing of the samples affect only the 5th
592 or even the 6th digit after the decimal point of the X_S values.
593
594

TABLE 2. Sulfur fugacities over solid pyrrhotite and unsaturated Fe-S melts (simple linear approximations (1100°C; 1400°C at low X_S) and equation [10] (1200, 1300°C; 1400°C at high X_S). Note: Equation [4] - has to be used to calculate sulfur fugacities over iron saturated Fe-S melts, see text)

T [°C]		Range X_S
1100, sol	$\log fS_2 = -98.01(\pm2.5) + 186.34(\pm4.9) \cdot X_S$	0.503 to 0.527
1100, liq	$\log fS_2 = -18.85(\pm1.2) + 30.01(\pm2.7) \cdot X_S$	0.423 to 0.475
1200 *	$\log fS_2 = 100.16(\pm15.49) + 2 \cdot \log X_S + 2 \cdot (1\text{-}X_S)^2 \cdot [-747.63(\pm161.90) + 2 \cdot 755.68(\pm200.60) \cdot (1\text{-}X_S) - 3 \cdot 282.16(\pm92.87) \cdot (1\text{-}X_S)^2]$	0.392 to 0.530
1300 †	$\log fS_2 = 82.4(\pm14.1) + 2 \cdot \log X_S + 2 \cdot (1\text{-}X_S)^2 \cdot [-631.31(\pm133.00) + 2 \cdot 655.81(\pm155.60) \cdot (1\text{-}X_S) - 3 \cdot 255.27(\pm67.80) \cdot (1\text{-}X_S)^2]$	0.325 to 0.53
1400	$\log fS_2 = -4.784(\pm0.031) + 0.8537(\pm0.1288) \cdot X_S$	0.125 to 0.38
1400	$\log fS_2 = 61.92(\pm2.36) + 2 \cdot \log X_S + 2 \cdot (1\text{-}X_S)^2 \cdot [-427.40(\pm18.95) + 2 \cdot 411.71(\pm19.96) \cdot (1\text{-}X_S) - 3 \cdot 146.02(\pm7.63) \cdot (1\text{-}X_S)^2]$	0.380 to 0.53

Fits use all literature data (see figure 2), except for: * literature data without Nagamori et al. (1970); † literature data without Nagamori et al. (1970) but including our results.

601 **Figure captions**

602

603 **Figure 1**

604 (A) Fe-S phase relationships as a function of temperature after Kubaschewski (1982).

605 (B) Sulfur fugacities over iron-saturated melts as function of temperature. These sulfur fugacities
606 can be calculated from equation [4], shown as the solid line in the Figure. Data are taken from
607 Bale and Toguri (1976, squares), Bog and Rosenqvist (1958, circles), Nagamori et al. (1970,
608 triangles), Sharma and Chang (1979, open hexagon), Chuang et al. (1985, open circle),
609 Rosenqvist and Dunicz (1952, circles semi-filled bottom), and Rosenqvist (1954, circles semi-
610 filled top).

611 Note: S_2 vapor is present in all stability fields as an additional phase.

612

613 **Figure 2**

614 Experimental data for sulfur fugacity as function of the mole fraction of sulfur at temperatures of
615 1100°C, 1200°C, 1300°C, and 1400°C. Data of the present work are plotted as closed circles.
616 Sulfur mole fractions in the Fe-S monitor are determined by the combustion method. The
617 uncertainties of the mole fraction of sulfur are within the symbol size. Sulfur fugacities are
618 calculated using thermodynamic data from Chase et al. (1998). Experiment S-IV-16 (1400°C) is
619 not plotted in the Figure. The fS_2 at X_S=0.125 (1400°C) equals the value of the intersect of the
620 dotted line with the y-axis. The vertical lines in the diagrams show the phase boundaries from the
621 phase diagram (Kubaschewski 1982). The stable phases are indicated and in addition S_2 vapor is
622 present with all phases. The dotted lines are best fit lines through the data (see text for more
623 details and Table 2). Please note that at high log fS_2 (0 to -1) the X_S does not depend on
624 temperature. At lower fS_2 deviations become prominent. The shape of the curves implies that a
625 small error in X_S has little effect on fS_2 determination of X_S values < 0.45 and has a more
626 pronounced effect for X_S values > 0.45.
627 Literature data: Bale and Toguri (1976, squares), Bog and Rosenqvist (1958, crossed circles),
628 Burgmann et al. (1968, circles), Ditman and Vecko (1965, diamonds), and Nagamori et al. (1970,
629 triangles).

630

631 **Figure 3A-C**

632 Comparison of oxygen fugacity determination by different methods. In all plots, the solid line
633 indicates the expected 1:1 correlation. The dotted lines are 1 % (Fig 3A) and 5 % (Fig 3B and 3C)
634 deviations from the 1:1 correlation. (A) Oxygen fugacities calculated using thermodynamic data
635 from Chase et al. (1998) vs. those using thermodynamic properties from Gurvich et al. (1989).
636 (B) Oxygen fugacities measured with solid state electrolyte sensors vs. fO_2 calculated using
637 thermodynamic data from Chase et al. (1998). (C) Oxygen fugacities measured with solid state
638 electrolyte sensors vs. fO_2 calculated using the thermodynamic data from Gurvich et al. (1989).

639

640 **Figure 4A-C**

641 (A) Sulfur fugacity calculated from the thermodynamic data from Chase et al. (1998) vs. sulfur
642 fugacity calculated using data from Gurvich et al. (1989). The solid line is the expected 1:1
643 correlation. The dotted line indicates 5 % deviations from the 1:1 line.

644 (B) Sulfur mole fractions in the Fe-S monitor determined by the weighing method vs. those
645 obtained from combustion method. The uncertainties of the calculated mole fraction of sulfur are
646 within the symbol size. The solid line is 1:1 correlation; the dotted lines indicate 5 % (black line)
647 and 15 % (grey line) deviations from the 1:1 line. #1: S-I-16, #2: S-I-18, #3: S-II-8, #4: S-I-11,
648 #5: S-IV-16. The deviations in X_S are larger for smaller sample sizes (see text).
649 (C) Sulfur fugacity calculated from the thermodynamic data from Chase et al. (1998) vs. sulfur
650 fugacity calculated using equation [10] and our experimental X_S data obtained from combustion
651 method. Only data at 1200°C and 1400°C are compared (see text for more details). The solid line
652 is 1:1 correlation; the dotted lines indicate 10 % (black line) and 15 % (grey line) deviations from
653 the 1:1 line.

This is a preprint, the final version is subject to change, of the American Mineralogist (MSA)
Cite as Authors (Year) Title. American Mineralogist, in press.
(DOI will not work until issue is live.) DOI: http://dx.doi.org/10.2138/am.2014.4376

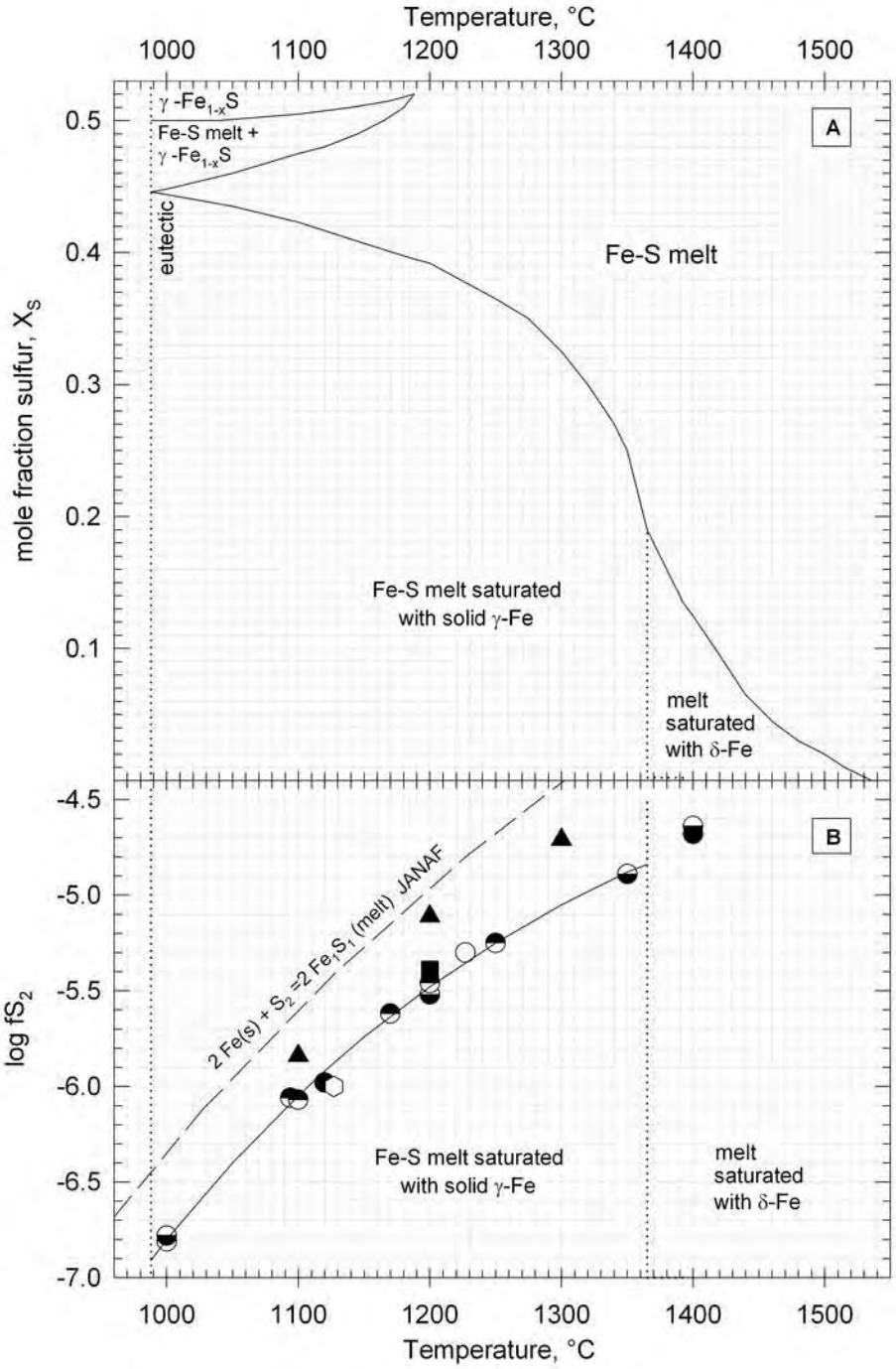

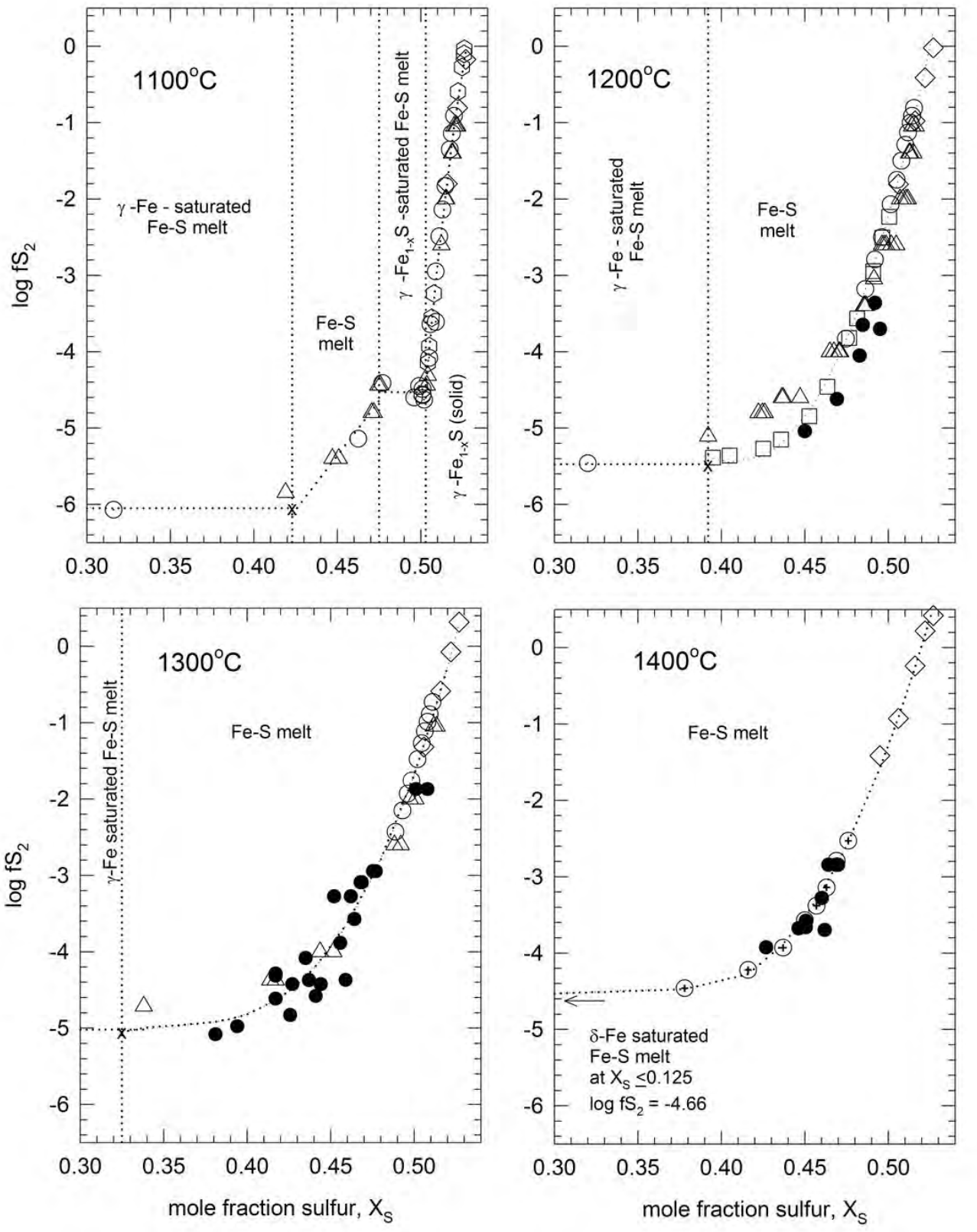
1100°C
γ -Fe - saturated Fe-S melt
Fe-S melt
γ -Fe1-xS -saturated Fe-S melt
γ -Fe1-xS (solid)
1200°C
γ -Fe - saturated Fe-S melt
Fe-S melt
1300°C
γ-Fe saturated Fe-S melt
Fe-S melt
1400°C
Fe-S melt
δ-Fe saturated Fe-S melt at XS ≤0.125
log fS2 = -4.66
log fS2
mole fraction sulfur, XS
0
-1
-2
-3
-4
-5
-6
0.30
0.35
0.40
0.45
0.50

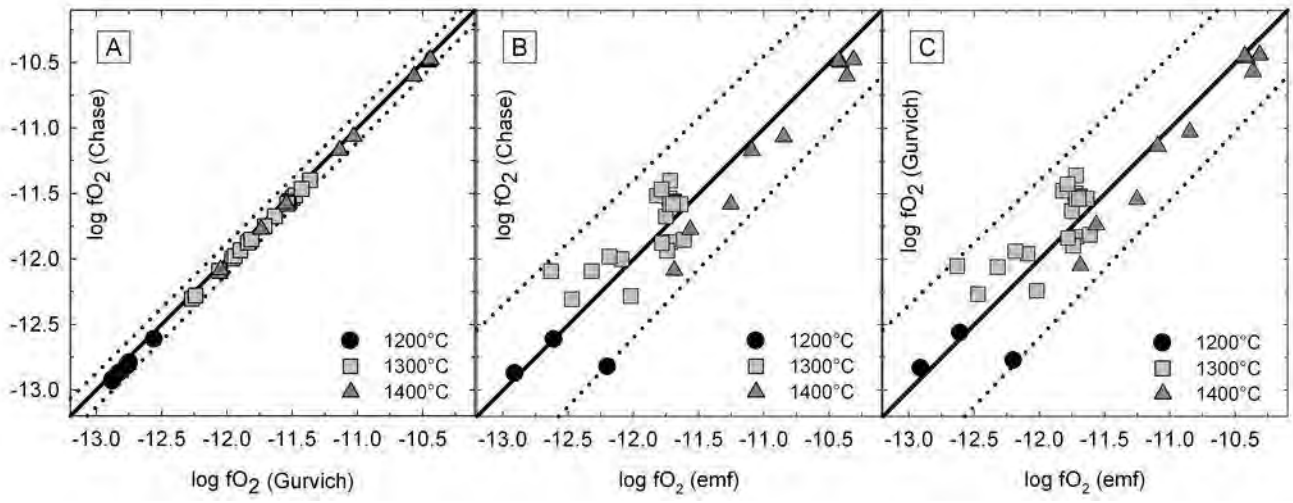
A
B
C
log fO2 (Chase)
log fO2 (Gurvich)
log fO2 (emf)
1200°C
1300°C
1400°C
-10.5
-11.0
-11.5
-12.0
-12.5
-13.0

This is a preprint, the final version is subject to change, of the American Mineralogist (MSA)
Cite as Authors (Year) Title. American Mineralogist, in press.
(DOI will not work until issue is live.) DOI: http://dx.doi.org/10.2138/am.2014.4376